Parallel Computational Ghost Imaging with Modulation Patterns Multiplexing and Permutation Inspired by Compound Eyes

Mengchao Ma,[1] Yinran Shen,[1] Peiyuan Zha,[1] Qingtian Guan,[1] Xiang Zhong,[1, a)] Huaxia Deng,[2, a)] Xuming Zhang,[3] and Ziwei Wang[4]

[1)]*Anhui Province Key Laboratory of Measuring Theory and Precision Instrument, School of Instrument Science and Opto-Electronics Engineering, Hefei University of Technology, Hefei, 230009, China.*

[2)]*CAS Key Laboratory of Mechanical Behavior and Design of Materials, Department of Modern Mechanics, University of Science and Technology of China, Hefei, Anhui 230027, China*

[3)]*Department of Applied Physics, The Hong Kong Polytechnic University, Kowloon, Hong Kong 999077, China*

[4)]*School of Engineering, Lancaster University, Lancaster, LA1 4YW, United Kingdom*

(Dated: 22 January 2024)

Real-time computational ghost imaging (CGI) has received significant attention in recent years to overcome the trade-off between long acquisition time and high reconstructed image quality of CGI. Inspired by compound eyes, we propose a parallel computational ghost imaging with modulation patterns multiplexing and permutation to achieve a faster and high-resolution CGI. With modulation patterns multiplexing and permutation, several small overlapping Fields of View (FOV) can be obtained, meanwhile the difficult in alignment of illumination light field and multiple detectors can be well resolved. The method combining compound eyes with multi-detectors to capture light intensity can resolve the issue of a gap between detector units in array detector. Parallel computation facilitates significantly reduced acquisition time while maintaining reconstructed quality without compromising sampling ratio. Experiments indicate that using $m \times m$ detectors reduce modulation pattern count, projector storage, and projection time to around $1/m^2$ of typical CGI methods, while increasing image resolution to m^2 times. This work greatly promotes the practicability of parallel computational ghost imaging and provides optional solution for real-time computational ghost imaging.

Real-time computational ghost imaging is a goal in optical imaging as it is becoming increasingly important in applications such as industrial measurement[1–6]. In theory, the reconstructed image composed of N pixels require N illumination light fields[7–10]. The number of illumination light fields grows in proportion to the number of pixels in the reconstructed image, resulting in a significant consumption of acquisition time. The long acquisition time is a major hindrance in real-time CGI.

Numerous studies in algorithm and hardware have been conducted to get around the long measurement time limitation. In terms of algorithms, CGI works well with compressive sensing(CS)[11–15], which is based on a mathematical iterative method. A N-pixel image can be reconstructed using less than N sub-patterns. Deep learning(DL) approaches[16,17] have also been developed to reduce illumination sub-pattern numbers. The modulation patterns number can be substantially reduced by CS and DL, while the reconstructed time may exceed the acquisition time at low sampling ratio. In terms of hardware, ultra-fast spatial light modulators[18,19] and parallel acquisition[20,21] are viable solutions for real-time imaging. Hahamovich et al.[19] demonstrated that a revolving structure and switched patterns can reach a modulation rate of 2.4 MHz by rotating the illumination sub-patterns.

Parallel acquisition provides more application scenarios and degree of freedom for CGI in large field-of-view imaging[22,23], shadow-free imaging[24,25]. Those method equivalent to the simultaneous implementation of multiple CGI processes in spatial domains. In each optical channel, it abides by the concept of a bucket detector. However, in parallel computational ghost imaging, the sub-pattern should be exactly received by each of the detection unit. The correspondence between the sub-patterns and the detection unit is difficult to determine when structured illumination is used. This situation may result in a seamed reconstructed image.

Inspired by the compound eyes of arthropod animals[26,27], we propose parallel computational ghost imaging with modulation patterns multiplexing and permutation. While array detectors have the issue of expensive manufacturing and a gap between detector units, our approach combines compound eyes with multi-detectors to capture light intensity. To resolve the difficulty in alignment of illumination sub-patterns and detectors, the approach of modulation patterns multiplexing and permutation is proposed. With modulation patterns multiplexing and permutation, several small overlapping FOV images can be obtained. A high-resolution and seamless image can be obtained by stitching sub-images from different FOVs. Therefore, the faster and high-resolution CGI can be achieved. This structure may be an alternative trade-off between the conventional camera and the single pixel camera in future.

CGI acquires image by a series of patterns interacting with the object. Then the spatial information of object is encoded into a 1-D light intensity measurements. This process is expressed as:

$$D_i = \sum_x \sum_y I_i(x,y) O(x,y) \tag{1}$$

where (x,y) denotes Cartesian coordinate, D_i is light intensity

[a)]Authors to whom correspondence should be addressed: Xiang Zhong, zhx0325@hfut.edu.cn; Huaxia Deng, hxdeng@ustc.edu.cn

measurements, $I_i(x,y)$ is illumination light field, $O(x,y)$ is the object, i is the ith measurements, $i = 1,2,3,\ldots,N$.

The large number of illumination light fields results in long time consumption and restricts the applications of CGI. Inspired by compound eyes, a parallel computational ghost imaging strategy is proposed as one possible solution.

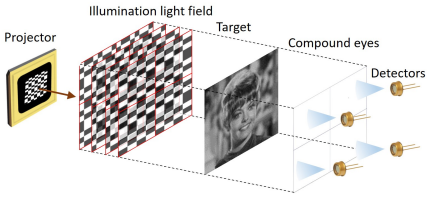

FIG. 1. Imaging principle of parallel computational ghost imaging.

The imaging principle of parallel computational ghost imaging is shown in Fig. 1. The compound eyes can be divided into two types according to the imaging principle: the apposition compound eyes and the superposition compound eyes[28–32]. The former can be regarded as a one-to-one relationship, while the latter can be considered as a one-to-many relationship[29]. Our work is inspired by the superposition compound eye[22], i.e., with limited number of detectors, a much higher image resolution than the number of detectors can be achieved. Similar to strepsipteran insects, the field-of-view of each microlens used in our system is subdivided into and represented by "chunks"[32], resulting to a sub-image of several thousand pixels.

In order to accomplish parallel computational ghost imaging, the illumination light field can be partitioned into a grid of m^2 small adjacent illumination sub-patterns. Since the encoding ability of the illumination sub-pattern remains intact, the encoding ability of the illumination light field is also unaffected after division. The parallel computational ghost imaging does not deviate from the essence of CGI since the system of multiple bucket detectors integrated with compound eyes has the same application scenarios as CGI and each FOV of compound eyes retains one single bucket detector.

It's easy to implement the illumination light field subdivision into multiple small adjacent non-overlapping illumination sub-patterns. As shown in Fig. 2, each sub-pattern interacts with the corresponding sub-region of object as:

$$D_i^j = \sum_x \sum_y I_i^j(x,y) O^j(x,y) \tag{2}$$

where $I_i^j(x,y)$ is the jth sub-pattern in the ith illumination light field, O^j is the jth sub-region of the object, and the 1-D light intensity measurements D_i^j for each sub-pattern are obtained by multiple detectors. The area covered by one sub-pattern is the FOV of one detector.

For example, suppose the object is divided into four sub-regions. $I^1(x,y)$, $I^2(x,y)$, $I^3(x,y)$, $I^4(x,y)$ are four non-overlapping sub-patterns denoted by different colours in

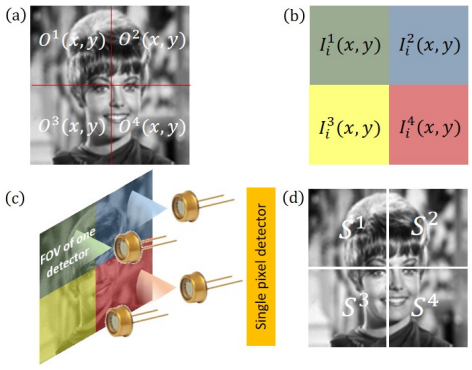

FIG. 2. The prospective flawless parallel ghost imaging result with non-overlapping modulation strategy with simulation. (a) The target object is divided into four areas. (b) Illumination light field consists of four sub-patterns. (c) The object illuminated by the light field. Each area is covered by one sub-pattern, and precisely coincides with the FOV of one detector. (d) The reconstructed sub-image of each illumination sub-pattern.

Fig. 2(b). $O^1(x,y)$, $O^2(x,y)$, $O^3(x,y)$, $O^4(x,y)$ are the target object precisely covered by four sub-patterns, respectively. Theoretically, the FOV of these sub-images are non-overlapping and aligned with each other perfectly, as shown in Fig. 2(d). Consequently, a prospective seamless stitched image can be obtained.

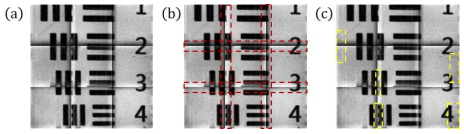

FIG. 3. The flawed parallel ghost imaging result with non-overlapping modulation strategy in practical experiments. (a) Stitched image. (b) Partial information loss in red dashed line. (c) Artifacts of some pixels in yellow dashed line

However, in practice, this non-overlapping subdivision of the illumination pattern is problematic. Non-overlapping between sub-patterns will result in a difficulty in alignment of illumination sub-patterns and the detectors. Then the crosstalk will occur in the reconstructed image. As shown in Fig. 3(a), the FOV of each detector can hardly detect precisely only one sub-pattern, resulting in obvious seam and flaw between the sub-images.

One solution to the aforementioned challenge is to achieve global consistency and correct alignment of the sub-images with overlapped FOV, which should be realized by overlapping modulation strategy in CGI systems.

Essentially, CGI recovers the image with light field modulation of a scene. The FOVs of the sub-images are determined by the sub-patterns. Therefore, the FOV overlapping

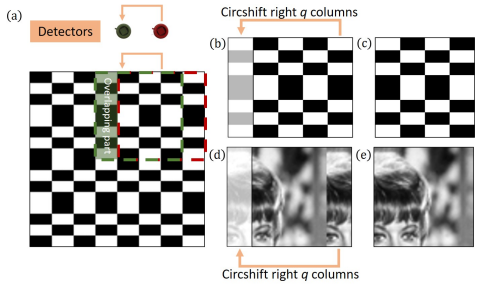

FIG. 4. The illustration of the permutation illumination sub-pattern and the sub-images displacement effect caused by modulation permutation. (a) Illumination light field composed of 4 Hadamard basis illumination sub-patterns. (b) Hadamard basis illumination sub-pattern. (c) Permutation illumination sub-pattern. (d) Displacement of the reconstructed image. (e) Displacement elimination with pixel permutation.

of sub-images is realized by overlapping of illumination sub-patterns. One natural way to realize illumination sub-patterns overlapping is to change the position of detector, as shown in Fig. 4(a). Original area received by red detector is denoted by red dotted line and new area received by green detector is denoted by green dotted line. The illumination sub-pattern that obtained by changing the position of the detector is actually a permutation of the illumination sub-patterns. The illumination sub-pattern received by above detectors are shown in Fig. 4(b) and (c). Compared with basis illumination sub-pattern, the permutation illumination sub-pattern is shifted right by q columns. The shift in sub-pattern can be expressed as:

$$I = \text{circshift}\left(I^1, [p, q]\right) \tag{3}$$

where circshift is the circular shift operation of the row / column exchanged, I is the permutation illumination sub-pattern, I^1 is the Hadamard basis illumination sub-pattern, p (q) is the number shifted up / down (left / right) where positive numbers represent shifted down (right).

Many different modulations can be used to permutate the patterns, including Hadamard basis modulation and Fourier basis modulation. A simulation with the permutation sub-patterns in Fig. 4(c) was performed and the imaging result was depicted in Fig. 4(d). It's evident that the reconstructed image is shifted leftward by q columns. The reconstructed image should have the same permutation as the permutation sub-pattern to avoid erroneous displacement, as shown in Fig. 4(e). The reconstructed image without displacement is called permutated image. Thus, the permutated image can be obtained if the permutation numbers of the sub-pattern is known.

As shown in Fig. 5, the FOV are divided into four parts, and the overlapped parts of the illumination sub-patterns are multiplexed as Fig. 5(a), thus overlapping sub-images can be obtained, as is shown in Fig. 5(b). Due to the permutation in basis illumination sub-pattern, the pixel positions of the reconstructed sub-images are displaced. It can be found from above procedures that multiplexing in illumination sub-pattern is equivalent to the permutation in the illumination sub-pattern which is achieved by the change in detector position.

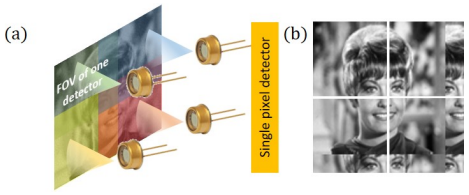

FIG. 5. Imaging with FOV overlapping of parallel computational ghost imaging leads to pixels displacement and flawed stitched image. (a) The illumination light field composed of multi-illumination sub-pattern that multiplexing between each illumination sub-pattern. (b) The pixel displacement of the sub-images.

While adjusting the detector location quantitatively is difficult in reality, the multiplexing numbers of the column / row of the basis illumination sub-pattern can be predetermined. As a result, the detectors' location can be identified accordingly.

The imaging principle of parallel computational ghost imaging with overlapping modulation is shown in Fig. 6. The projector's illumination patterns differ from Fig. 1 in that they are multiplexed rather than non-overlapping. The multiplexed parts are located in the colour overlay areas. These parts are shared by the surrounding illumination sub-patterns and the surrounding detectors. The compound eyes are used for collecting light intensity measurements for multiple detectors. The lens number of the compound eyes should be the same as the illumination sub-pattern numbers. Without loss of generality, the illumination light field are subdivided into four sub-patterns and 16 pixels are multiplexed among them. The total number of the illumination patterns is 4096.

The reconstructed sub-images with different illumination sub-patterns are shown in Fig. 7(b). The image reconstruction process can be expressed as:

$$S^j = \mathscr{H}^{-1}\left\{D^j\right\} \tag{4}$$

where $\mathscr{H}^{-1}$ denotes inverse Hadamard transform, D^j is the 1-

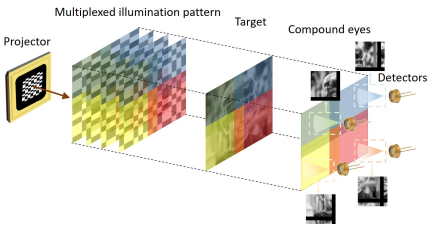

FIG. 6. Imaging principle of parallel computational ghost imaging via multiplexed modulation. The Field of View of different detectors are denoted by different colours.

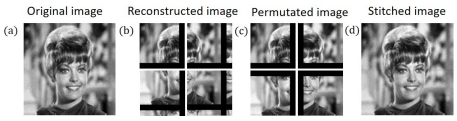

FIG. 7. Simulation result. (a) The original image. (b) The reconstructed image of each illumination sub-pattern. (c) The permutated image of each illumination sub-pattern. (d) The stitched image.

D light intensity measurement for each sub-pattern, S^j is the reconstructed sub-image of corresponding sub-pattern. The reconstructed sub-images exhibit evident black regions because the multiplexed parts can not be fully accepted by the detectors. Nevertheless, the light intensity of black regions can be accepted by the surrounding detectors. Therefore, the black regions have no influence on the stitched image. In addition to the black areas, the reconstructed sub-images also manifest apparent displacement from the original image. This displacement can be eliminated by pixels permutations and the permutated images are shown in Fig. 7(c). The elimination method with pixels permutation can be expressed as:

$$T^j = \text{circshift}\left(S^j, [m,n]\right) \tag{5}$$

where T^j is the permutation image that has been eliminated displacement by pixels permutations, $m(n)$ is the number shifted same as the corresponding sub-pattern. Finally, the stitched image of 112×112 pixels is obtained by stitching the permutated image together according to the permutation number of the illumination pattern. Due to multiplexing of some of the pixels, the stitched resolution is a little bit smaller than 128×128 pixels.

Notably, because the permutation amount is predetermined, stitching the images only requires a simple sum of the pixels in the multiplexed sections and does not require any complicated methods. This could be an additional benefit of the proposed parallel ghost imaging method with modulation multiplexing and permutation.

The feasibility of the proposed method is verified by experiments. Fig. 8 depicts the experimental setup schematic. The system comprises of a projector(DLP7000) with a resolution of 1024×768 pixels, nine detectors, a large condense lens, and compound eyes(9 lenses). Multiplexed patterns are generated using 9 Hadamard basis sub-patterns with a resolution of 64×64 pixels. There are 16 pixels of column / row multiplexing. The multiplexed patterns is of 160×160 pixels and the total number is 4096.

The projector is programmed to run at 1000 frames per second. The correlation between the multiplexed patterns and the compound eyes should be set to guarantee that the multiplexed regions can be shared with the surrounding detectors.

Both transmissive and reflective configurations are feasible for multiplexing CGI. The experiment setup of transmissive configuration is shown in Fig. 8(a). We should include the edge of each lens of the compound eyes in the multiplexed part. After the multiplexed illumination pattern interacting with the object, modulated light field is received by compound

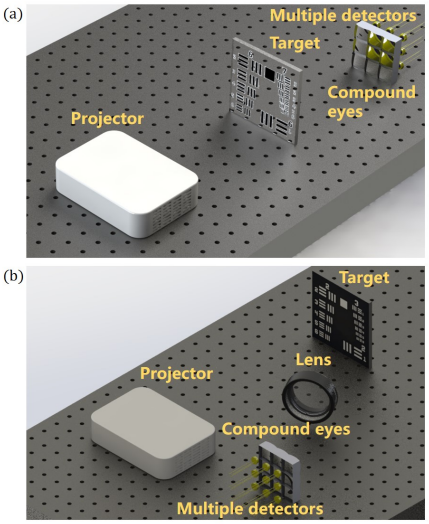

FIG. 8. Experimental setup. (a) Transmissive experimental setup. (b) Reflective experimental setup.

eyes (8.4cm $\times$ 8.4cm). The signals of detectors is simultaneously recorded by DAQ(data acquisition device).

In the first column of Fig. 9(b), the original photographs are displayed. In the second column of Fig. 9(b), the reconstructed sub-images are of 64×64 pixels. The pixel coordinates of the reconstructed sub-images are changed based on the permutation of the multiplexed sub-patterns and the basis sub-patterns. The permutated sub-images are then obtained, as illustrated in the third column of Fig. 9(b). The permuted sub-images are eventually merged together to produce a stitched image of 160×160 pixels, as illustrated in the fourth column of Fig. 9(b).

Furthermore, as illustrated in the last column of Fig. 9(b), the conventional non-overlapping approach introduces considerable defects between the stitched portions of the sub-images. While the overlapping approach with pattern multiplexing and permutation is completely devoid of apparent stitching gaps.

The experiment setup of reflective configuration is shown in Fig. 8(b). Since the compound eyes and the detectors have to be placed much farther than the transmission case to avoid the interference of the illumination patterns, a condense lens is placed on between the target and the compound eyes to restrict the reflected light to be effectively collected by each of the corresponding detectors while avoid the crosstalk of reflected light from the adjacent microlenses(see Sec.1 in the supplementary material for a full description). The results are shown in Fig. 9(a)(see Sec.2 in the supplementary material for more experimental results). The second column and third column in Fig. 9(a) are reconstructed sub-images and permu-

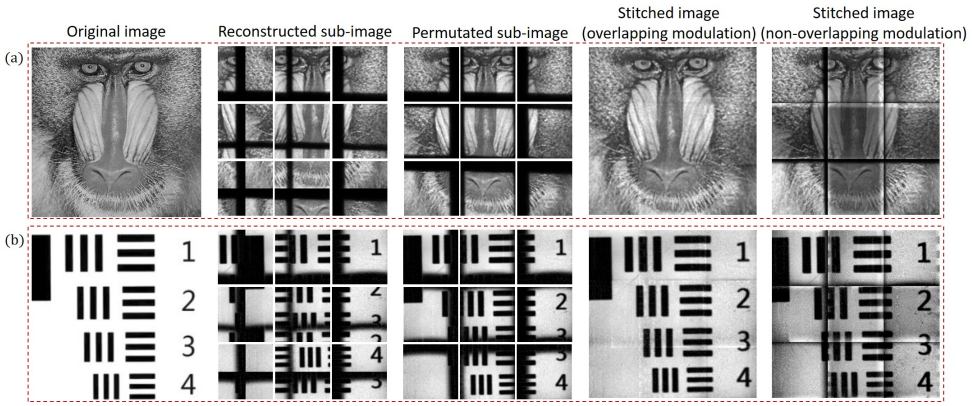

FIG. 9. Experimental result with reflective and transmissive experimental setup. (a) is the experimental result of reflective experimental setup. (b) is the experimental result of transmissive experimental setup.

tated sub-images, respectively. The stitched image with 160 × 160 pixels is obtained by stitching the permutated sub-images, as shown in the fourth column of Fig. 9. The comparison of the stitched image between overlapping modulation and non-overlapping modulation is shown in the fourth column and the last column of Fig. 9, respectively.

With the proposed multiplexing strategy, the number of the illumination patterns are significantly decreased, thus the required storage memory of the projector and the acquisition time are also decreased(see Sec.3 in the supplementary material for a full description).

High-resolution image reconstruction studies serve as further confirmation of the benefit of the suggested parallel CGI. The set up resembles Fig. 8(b). The size of each sub-pattern is 256×256 pixels. According to Fig. 10, the stitched image resolution can be as high as 640×640 pixels.

Notably, traditional CGI uses up to 409600 modulation patterns. Due to the projector's limited on-board memory, a huge number of patterns are not viable (more than 38 giga bytes).

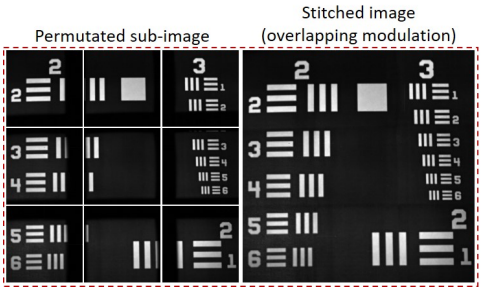

FIG. 10. High resolution(640 × 640 pixels) imaging result.

While parallel CGI takes only 6 giga bytes(65536 modulation patterns). Furthermore, the projection and acquisition times are excessive. CGI takes about 409.6 seconds to rebuild one image at 1000 frames per second, but 65.5 seconds using the suggested method.

In conclusion, this research developed a parallel computational ghost imaging approach featuring modulation pattern multiplexing and permutation to improve imaging speed and resolution. The method of modulation patterns multiplexing and permutation corrects the alignment of illumination pattern and multiple detectors. The issue of a gap between detector units can be resolved by multiple detectors combining with compound eyes. The simultaneous acquisition of small overlapping FOVs allows for fast imaging speed without compromising reconstructed quality or sampling ratio. Experiments demonstrated that parallel computational ghost imaging strategy can produce seamless image of higher resolution than each sub-image by stitching nine reconstructed sub-images from different FOVs. This work provides an enormous enlightening for real-time ghost imaging, wide field-of-view imaging and other applications.

See the supplementary material for details of the illustration of the storage consumed in projector and the time consumption, the experiment result with different objects, the reasons for requiring a condense lens in the reflective configuration.

ACKNOWLEDGMENTS

This work is supported by National Natural Science Foundation of China (Grant Nos. 52275529 and 12372187), Natural Science Foundation of Anhui Province(1908085J15 and 2208085ME138), Fundamental Research Funds for the Central Universities (WK2090000039, WK2480000010), and CAS Talent Introduction Program (KY2090000077).

AUTHOR DECLARATIONS

Conflict of Interest

The authors declare no conflicts of interest.

Author Contributions

Mengchao Ma: Conceptualization (equal); Funding acquisition (equal); Software (equal); Validation (equal); Visualization (equal); Writing - original draft (equal); Writing – review & editing (equal). **Yinran Shen**: Conceptualization (equal); Software (equal); Validation (equal); Visualization (equal); Writing - original draft (equal); Writing – review & editing (equal). **Peiyuan Zha**: Validation (equal); Visualization (equal). **Qingtian Guan**: Validation (equal); Visualization (equal). **Xiang Zhong**: Funding acquisition (equal); Validation (supporting). **Huaxia Deng**: Conceptualization (equal); Funding acquisition (equal); Writing – original draft (equal); Writing – review & editing (equal). **Xuming Zhang**: Supervision (equal); Writing – review & editing (equal). **Ziwei Wang**: Validation (equal); Writing – review & editing (equal).

DATA AVAILABILITY STATEMENT

The data that support the findings of this study are available from the corresponding author upon reasonable request.

[1]H. Li, W. Hou, Z. Ye, T. Yuan, S. Shao, J. Xiong, T. Sun, and X. Sun, "Resolution-enhanced x-ray ghost imaging with polycapillary optics," APPLIED PHYSICS LETTERS **123** (2023), 10.1063/5.0168704.
[2]V. Cecconi, V. Kumar, A. Pasquazi, J. Totero Gongora, and M. Peccianti, "Nonlinear field-control of terahertz waves in random media for spatiotemporal focusing [version 3; peer review: 2 approved]," Open Research Europe **2** (2023), 10.12688/openreseurope.14508.3.
[3]L. Leibov, A. Ismagilov, V. Zalipaev, B. Nasedkin, Y. Grachev, N. Petrov, and A. Tcypkin, "Speckle patterns formed by broadband terahertz radiation and their applications for ghost imaging," SCIENTIFIC REPORTS **11** (2021), 10.1038/s41598-021-99508-1.
[4]L. Olivieri, J. S. T. Gongora, A. Pasquazi, and M. Peccianti, "Time-resolved nonlinear ghost imaging," ACS PHOTONICS **5**, 3379–3388 (2018).
[5]D. Yang, C. Chang, G. Wu, B. Luo, and L. Yin, "Compressive ghost imaging of the moving object using the low-order moments," APPLIED SCIENCES-BASEL **10** (2020), 10.3390/app10217941.
[6]L. Zhou, Y. Xiao, and W. Chen, "Edge detection in gradient ghost imaging through complex media," APPLIED PHYSICS LETTERS **123** (2023), 10.1063/5.0166946.
[7]G. M. Gibson, S. D. Johnson, and M. J. Padgett, "Single-pixel imaging 12 years on: a review," OPTICS EXPRESS **28**, 28190–28208 (2020).
[8]M. P. Edgar, G. M. Gibson, and M. J. Padgett, "Principles and prospects for single-pixel imaging," NATURE PHOTONICS **13**, 13–20 (2019).
[9]Z. Zhang, X. Wang, G. Zheng, and J. Zhong, "Hadamard single-pixel imaging versus fourier single-pixel imaging," OPTICS EXPRESS **25**, 19619–19639 (2017).
[10]L.-K. Du, S. Sun, L. Jiang, C. Chang, H.-Z. Lin, and W. T. Liu, "Information segregating towards simultaneous tracking and imaging based on ghost imaging," PHYSICAL REVIEW APPLIED **19** (2023), 10.1103/PhysRevApplied.19.054014.
[11]J.-T. Ye, C. Yu, W. Li, Z.-P. Li, H. Lu, R. Zhang, J. Zhang, F. Xu, and J.-W. Pan, "Ultraviolet photon-counting single-pixel imaging," APPLIED PHYSICS LETTERS **123** (2023), 10.1063/5.0157862.
[12]M. F. Duarte, M. A. Davenport, D. Takhar, J. N. Laska, T. Sun, K. F. Kelly, and R. G. Baraniuk, "Single-pixel imaging via compressive sampling," IEEE SIGNAL PROCESSING MAGAZINE **25**, 83–91 (2008).
[13]C. A. Metzler, A. Maleki, and R. G. Baraniuk, "From denoising to compressed sensing," IEEE TRANSACTIONS ON INFORMATION THEORY **62**, 5117–5144 (2016).
[14]O. Katz, Y. Bromberg, and Y. Silberberg, "Compressive ghost imaging," APPLIED PHYSICS LETTERS **95** (2009), 10.1063/1.3238296.
[15]J. H. Shapiro, "Computational ghost imaging," PHYSICAL REVIEW A **78** (2008), 10.1103/PhysRevA.78.061802.
[16]X. Liu, T. Han, C. Zhou, J. Hu, M. Ju, B. Xu, and L. Song, "Computational ghost imaging based on array sampling," OPTICS EXPRESS **29**, 42772–42786 (2021).
[17]C. Zhou, X. Liu, Y. Feng, X. Li, G. Wang, H. Sun, H. Huang, and L. Song, "Real-time physical compression computational ghost imaging based on array spatial light field modulation and deep learning," OPTICS AND LASERS IN ENGINEERING **156** (2022), 10.1016/j.optlaseng.2022.107101.
[18]Z.-H. Xu, W. Chen, J. Penuelas, M. Padgett, and M.-J. Sun, "1000 fps computational ghost imaging using led-based structured illumination," OPTICS EXPRESS **26**, 2427–2434 (2018).
[19]E. Hahamovich, S. Monin, Y. Hazan, and A. Rosenthal, "Single pixel imaging at megahertz switching rates via cyclic hadamard masks," NATURE COMMUNICATIONS **12** (2021), 10.1038/s41467-021-24850-x.
[20]M. A. Herman, J. Tidman, D. Hewitt, T. Weston, and L. McMackin, "A higher-speed compressive sensing camera through multi-diode design," in COMPRESSIVE SENSING II, Proceedings of SPIE, Vol. 8717, edited by F. Ahmad (SPIE, 2013) conference on Compressive Sensing II, Baltimore, MD, MAY 02-03, 2013.
[21]M.-J. Sun, H.-Y. Wang, and J.-Y. Huang, "Improving the performance of computational ghost imaging by using a quadrant detector and digital micro-scanning," SCIENTIFIC REPORTS **9** (2019), 10.1038/s41598-019-40798-x.
[22]M. Ma, Y. Zhang, H. Deng, X. Gao, L. Gu, Q. Sun, Y. Su, and X. Zhong, "Super-resolution and super-robust single-pixel superposition compound eye," OPTICS AND LASERS IN ENGINEERING **146** (2021), 10.1016/j.optlaseng.2021.106699.
[23]Z. Ji, Y. Liu, and X. Chen, "Mosaic-free compound eye camera based on multidirectional photodetectors and single-pixel imaging," OPTICS LETTERS **47**, 6349–6352 (2022).
[24]M. Ma, Q. Sun, X. Gao, H. Deng, G. Wang, Y. Su, Q. Guan, and X. Zhong, "Single-pixel imaging in the presence of specular reflections," APPLIED OPTICS **60**, 2633–2639 (2021).
[25]S. Li, Z. Zhang, X. Ma, and J. Zhong, "Shadow-free single-pixel imaging," OPTICS COMMUNICATIONS **403**, 257–261 (2017).
[26]Z. Ji, Y. Liu, C. Zhao, Z. L. Wang, and W. Mai, "Perovskite wide-angle field-of-view camera," ADVANCED MATERIALS **34** (2022), 10.1002/adma.202206957.
[27]Q. Fan, W. Xu, X. Hu, W. Zhu, T. Yue, C. Zhang, F. Yan, L. Chen, H. J. Lezec, Y. Lu, A. Agrawal, and T. Xu, "Trilobite-inspired neural nanophotonic light-field camera with extreme depth-of-field," NATURE COMMUNICATIONS **13** (2022), 10.1038/s41467-022-29568-y.
[28]C. J. van der Kooi, D. G. Stavenga, K. Arikawa, G. Belusic, and A. Kelber, "Evolution of insect color vision: From spectral sensitivity to visual ecology," in ANNUAL REVIEW OF ENTOMOLOGY, VOL 66, 2021, Annual Review of Entomology, Vol. 66, edited by A. Douglas (2021) pp. 435–461.
[29]S. Wu, T. Jiang, G. Zhang, B. Schoenemann, F. Neri, M. Zhu, C. Bu, J. Han, and K.-D. Kuhnert, "Artificial compound eye: a survey of the state-of-the-art," ARTIFICIAL INTELLIGENCE REVIEW **48**, 573–603 (2017).
[30]A. Borst and J. Plett, "Seeing the world through an insect's eyes," NATURE **497**, 47–48 (2013).
[31]Y. M. Song, Y. Xie, V. Malyarchuk, J. Xiao, I. Jung, K.-J. Choi, Z. Liu, H. Park, C. Lu, R.-H. Kim, R. Li, K. B. Crozier, Y. Huang, and J. A. Rogers, "Digital cameras with designs inspired by the arthropod eye," NATURE **497**, 95–99 (2013).
[32]E. Buschbeck, B. Ehmer, and R. Hoy, "Chunk versus point sampling: Visual imaging in a small insect," Science **286**, 1178–1180 (1999), https://www.science.org/doi/pdf/10.1126/science.286.5442.1178.